Optica Applicata, Vol. XLV, No. 3, 2015
DOI: 10.5277/oa150306

All-optical sensor based on nonlinear multimode interference coupler features

MEHDI TAJALDINI[1, 2*], MOHD Z.M. JAFRI[1]

[1]School of Physics, University Sains Malaysia, 11800 Penang, Malaysia

[2]Department of Mathematics, Baft Branch, Islamic Azad University, Baft, Iran

[*]Corresponding author: tajaldini.usm@gmail.com

In this study, we investigate the sensing applications in the presence of the nonlinear effects by proposing an all-optical sensor and considering nonlinear effects on modal propagation and output intensity based on an ultra-compact nonlinear multimode interference coupler. The sensor can be tuned to have the highest sensitivity in the wavelength and refractive index ranges and can detect water-soluble chemicals, air-pollutions, earthquake wave, blood parameters, and heart operation. The results indicate high output sensitivity to input wavelength whereas the nonlinear effects appear in the medium. This sensitivity led us to propose a wave sensor of both transverse and longitudinal waves, such as acoustic and light waves, when an external wave interacts with an input waveguide. For instance, this sensor can be implemented using a long input that is inserted in the land, and any wave could then be detected from the Earth. The visible changes in intensity at the output facet in various refractive indices of the surrounding layer show the high sensitivity to the refractive index of the surrounding layer, which is the foundation of introducing a sensor. Generally, the results show the high efficiency of nonlinear effects in all-optical sensing performances.

Keywords: nonlinear multimode interference (NLMMI), nonlinear modal propagation analysis (NMPA), all-optical sensor, cladding refractive, chemical sensing, earthquake, air pollution, water-soluble.

1. Introduction

Multimode interference (MMI) couplers [1] have recently become key elements in planar integrated photonics. These couplers have significant features such as low loss and crosstalk [2], high optical bandwidth [3], compact size [4], low sensitivity to input polarization [5], low sensitivity to operating wavelength [6], and tolerance to fabrication errors. MMI couplers have broad applications in photonic complex circuits. An important application is an all-optical sensor, especially when operated in the nonlinear regime.

MMI couplers have been widely used for various sensing purposes, such as temperature, pressure, and chemical/biological sensors, in which the change in refractive index is indicative of the change in output intensity [7–9]. Several MMI sensors have been introduced by changing their configuration to have a small length of self-imaging formation and they are also modeled to have a long length and complicated structures [9].

The NLMMI coupler as an active device is more sensitive to input characterization and region environment, which can change the interference mechanism among the guided modes. Nonlinear regimes might be more sensitive to the changes in parameters such as the refractive index of the surrounding and core layers, input wavelength and intensity produced by self- and cross-phase modulation, wave-mixing, and exchange energy among exited modes. Therefore, the NLMMI coupler has the potential to be an accurate sensor.

In this paper, the nonlinear modal propagation analysis (NMPA) [10–15] method is applied in multimode interference waveguide as a novel and high potential approach for detecting air pollution, water-soluble materials, and waves, which affect the input waveguide. Each change in the surrounding layer or input wavelength leads to an MMI reaction, which is demonstrated in modal propagation and output intensity. The high changes in output intensity created as a result of the variety of surrounding layers prove the high performance of the proposed sensor. Notably, this nonlinear device could demonstrate reaction to other stimuli such as light, acoustic wave, and temperature, as well as the change in the surrounding layer.

This paper is arranged as follows: in Section 2, NMPA is introduced and several nonlinear effects are explained. The results and discussions of the robust sensor are presented in Section 3. Finally, the conclusion and future directions of this research are shown in Section 4.

2. Nonlinear modal propagation analysis

The MMI coupler is introduced to photonic devices as having the simplest structure. Although this device has broad applications in integrated photonic circuits and telecommunications, its use has propagated with the appearance of nonlinear effects because of changes in the modes of the electric field in terms of amplitudes or phases. This application exchanges energy among modes [15]. This advantage leads to an ability to control the wave propagation in the medium, thereby contributing to signal processing in all-optical functions [13].

The central region of the MMI coupler is the multimode waveguide. The access waveguides that are usually in single mode are fixed at the input and output facets of the multimode waveguide (Fig. 1). The performance of these devices depends on the interference of guided modes, where the complete constructive interference contributes to the formation of single or multiple self-images at precise distances in the input facet. The interference property of the MMI waveguide significantly depends on the refractive indices of the core and cladding regions of the multimode waveguide. In other words, by varying the refractive index in the core or the cladding region, modal

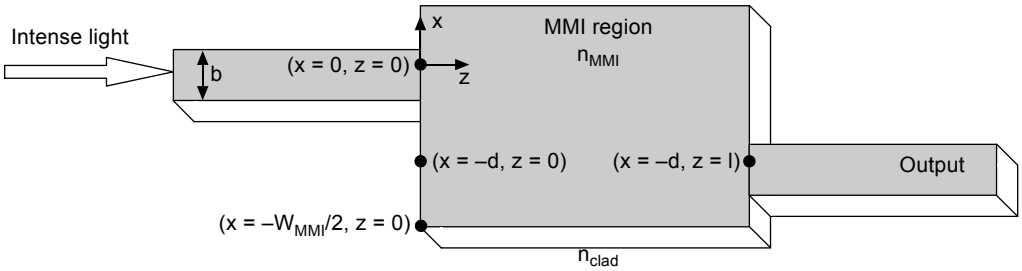

Fig. 1. Schematic structure of an MMI coupler.

interferences phenomena are also changed. In fact, by exposing the multimode region to intense light, the core refractive index becomes a function of intensity in the presence of the Kerr nonlinear effect. As a result, the modes propagate in a different manner according to changes in optical properties. We can design an all-optical sensor to have small MMIs by studying this effect in multimode interference couplers and by applying the obtained results. In this section, we theoretically study the nonlinear effects in an MMI coupler by studying the NMPA method in the central region.

The refractive index is shown in Fig. 2, and our design is shown as well. In fact, the MMI coupler is assumed as a conventional structure. Notably, n_{MMI} must be higher than n_{clad} to confine the light in the core region that originates from the total reflection basis.

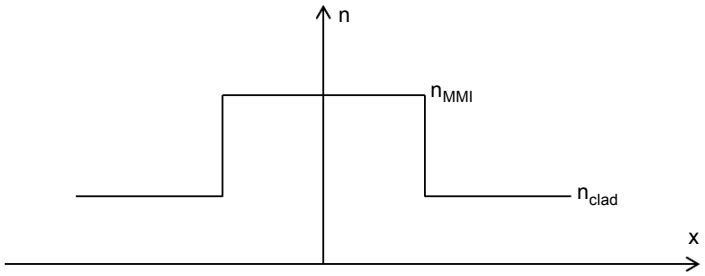

Fig. 2. Refractive index in a ridge waveguide.

The critical angle determines the mode expansion in the lateral direction and is dependent on the refractive indices of the core and cladding layer. When boundary conditions are used, the guided modes are discreet, which is consistent with the theory of optical waveguides. In other words, the critical angle indicates the guided mode number.

The MMI region is isotropic, and the field in this region is a superposition of all the modal fields of the MMI. The details of the modal propagation analysis (MPA) method are shown in [1, 16]. In studying the NMPA, the mode amplitudes are considered as a function of propagation direction and they not only show the phase and amplitude changes in the region but also the exchange of energy among modes (in the *z* direction). On the other hand, the amplitude of the modal fields is constant in the lin-

ear regime. Therefore, we follow the conventional MPA while considering the mode amplitudes as a function of propagation direction, and then the nonlinear coupled equations of guided modes are solved to obtain the electric field throughout the MMI region to apply the Kerr effect on MPA and to propose NMPA.

The height of the MMI coupler is considered to be 1 μm that leads to the excitation of a mode in vertical direction (y) so that a propagation constant is produced in this direction. The light distribution in 3D is expressed as

$$\psi(x, z, t) = \sum_{v=0}^{n} \varphi_v(z)\, e^{j\beta_v z} e^{j\gamma_v x} e^{jk_y y} e^{-\omega t + \phi_0} \tag{1}$$

After substituting the above equation in the nonlinear wave equation, the following equation is obtained

$$\sum_v \left[\frac{\mathrm{d}^2\varphi_v(z)}{\mathrm{d}z^2} + 2j\beta_v \frac{\mathrm{d}\varphi_v(z)}{\mathrm{d}z} - (\beta_v^2 + \gamma_v^2 + k_y^2)\varphi_v(z) + \frac{n^2\omega^2}{c^2}\varphi_v(z) \right] e^{j\gamma_v x} e^{j\beta_v z} e^{jk_y y} e^{-j\omega t} =$$

$$= \frac{3\chi_e^{(3)}\omega^2}{c^2} \sum_p \sum_q \sum_s \Big[\varphi_p \varphi_q \varphi_s^* e^{j(\gamma_p + \gamma_q - \gamma_s)x} e^{j(\beta_p + \beta_q - \beta_s)z} e^{-j\omega t} +$$

$$+ \varphi_p \varphi_q \varphi_s e^{j(\gamma_p + \gamma_q + \gamma_s)x} e^{j(\beta_p + \beta_q + \beta_s)z} e^{-j3\omega t} \Big] e^{jk_y y} \tag{2}$$

The second term in the left side of the equation indicates third-harmonic generation. The explained procedure in our study can be used for the third-harmonic generation by considering the mentioned term in solving the nonlinear coupled equations and in obtaining the modes electric field in the launched and generated frequency; however, because of the sensing application on the frequency ω (same frequency as the input), we avoid considering the third-harmonic generation and omit the related term.

From the above equation, we have a dispersion equation as:

$$\beta_v^2 + \gamma_v^2 + k_y^2 = n^2 k_0^2 \tag{3a}$$

$$\beta_v^2 + \gamma_v^2 = n^2 k_0^2 - k_y^2 = \left(n^2 - \frac{k_y^2}{k_0^2} \right) k_0^2 \tag{3b}$$

Comparing Eqs. (3a) and (3b), the effective refractive index for the core layer is obtained as

$$n_{\mathrm{MMI}} = \left(n^2 - \frac{k_y^2}{k_0^2} \right)^{1/2} \tag{4}$$

The core refractive index is affected by the surrounding layer refractive index, as shown in Eq. (4).

Notably, the penetration depth of each mode into the cladding region is very small and has a negligible effect on the device performance. Thus, the clad refractive index does not contribute to this effective refractive index. Moreover, the negligible penetration and single mode in the vertical direction enable the ease of the efective index method (EIM) procedure. In the above method, EIM is not an approximation against the other. Notably the vertical profile of the electric field does not change from the input waveguide to the MMI. As such, access waveguides should follow the MMI and be considered in 2D because they have 100% overlap in the y direction because they have the same mode in the y direction.

In fact, the electric field in the y direction is not affected by the nonlinear medium and as such, there is no need to indicate it in the electric field, which is why the medium is studied in 2D.

Therefore, the field distribution of the light in the MMI region is expressed by

$$E(x, z, t) = \sum_{v=0}^{n} A_v(z)\, e^{j\gamma_v x} e^{j\beta_v z} e^{-\omega t + \varphi_0} \tag{5}$$

where v is the mode number, $A_v(z)$ is the amplitude of the v-th mode that contains real and imaginary parts, γ_v and β_v are lateral and longitudinal propagation constants of the v-th mode, respectively. With the appearance of the nonlinear effect in the MMI region, the refractive index of this region changes and contains a nonlinear part. The total refractive index of the MMI region is then given by

$$n = n_{\mathrm{MMI}} + n_2 I = n_{\mathrm{MMI}} + n_{\mathrm{NL}} \tag{6}$$

where n_{MMI} is the usual weak-field refractive index of the guiding structure (linear term), I denotes the intensity of the input light, and n_{NL} is the nonlinear refractive index determined by the Kerr nonlinear effect.

Here, applying the NMPA is the most important process to study the nonlinear phenomenon, which is induced in the multimode waveguide that is launched with a linearly polarized wave. Such a phenomenon could induce several desirable effects on mode propagations and interactions, as discussed in the next section.

The nonlinear mode equation for the MMI coupler obtained from NMPA is (from Eq. (2) [13])

$$2j\beta_v \frac{\mathrm{d}\varphi_v(z)}{\mathrm{d}z} = -\frac{3\chi_e^{(3)}\omega^2}{c^2} \sum_p \sum_q \varphi_p \varphi_q \varphi_s^* C_v(p, q, s) \tag{7}$$

where $C_v(p, q)$ are the overlap coefficients of the different modes. Here, the right-hand side of Eq. (7) includes self-phase modulation terms ($p = q = v = s$), cross-phase modulation terms ($p = v \neq q = s$), and terms that lead to power exchange among the modes.

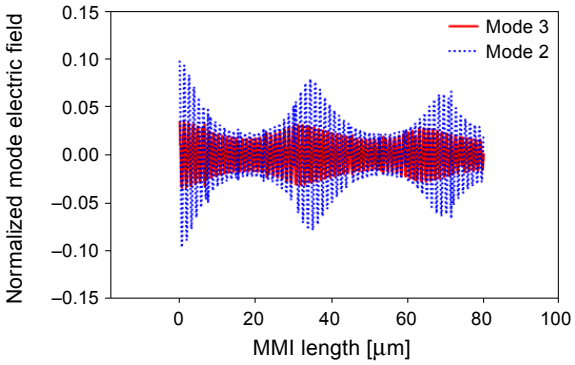

Fig. 3. Normalized electric field in MMI length.

This set of coupled numerical differential equations can be solved using high-accuracy Finite difference method (FDM) but is time consuming. Moreover, memory limitations restrict its application to small low-intensity nonlinear MMI.

By solving the set of v coupled equations of the field amplitudes ($v = 0, \pm1, \pm2, ...$), the field amplitude $A_v(z)$ of the modes is obtained. Consequently, by using Eq. (7), the field in the MMI region can be obtained; numerical calculations show the amplitudes as an interpolating function that are complex numbers.

For clarity, we used the results of self- and cross-phase modulation and wave-mixing from our last report on glass [15] and they are shown in Fig. 3.

In the self-phase modulation effect, the sinusoidal profile is converted to the Gaussian profile without change in the amplitude maximum (Fig. 3). However, changes in wavelength, amplitude maximum, and wavelength shift between two modes originate from cross-phase modulation and wave-mixing.

The field profile of the guided modes, in general, consists of a superposition of sine and cosine light waves, with zero fields at the boundaries of the guiding region. In addition, we assume that there is negligible penetration of the fields in the cladding layer as well as Goos–Hanchen shift because of the high contrast index, which increases by imposing nonlinearity.

The field amplitude in the output port is obtained by evaluating the summation of the overlap integral between the profile of an output waveguide and the profile of the excited modes of the MMI region

$$E_{0r,\,\mathrm{m},\,v} = \frac{\int A_v(L) e^{j\gamma_v x} \cos[k_x(x-(-1)^{m+1}d) + \phi_0]\,\mathrm{d}x}{\left\{\int \left|e^{j\gamma_v x}\right|^2 \mathrm{d}x \int \left|\cos[k_x(x-(-1)^{m+1}d) + \phi_0]\right|^2 \mathrm{d}x\right\}^{1/2}} \tag{8}$$

By calculating the summation of the above equation with regards to the outputs, the electric field in the output is obtained.

3. Results and discussion

Nonlinear effects in the multimode waveguide cause high sensitivity to physical parameters such as refractive indices, wavelength, phase, dimension, and input intensity. However, in linear regimes, multimode waveguides as passive do not have any reaction to every parameter, especially to the input intensity, whereas in nonlinear regime, they are active and have strong reaction to any changes either in the system or environment characteristics. The high sensitivity of output intensity to the surrounding layer and input wavelength and intensity give us an opportunity of producing excellent biological/chemical and geophysics sensors by studying an nonlinear multimode interference (NLMMI) coupler based on the NMPA method. Our study includes investigations of output intensity as a function of input intensity, input wavelength, and cladding refractive index (air and liquid categories). The mode expansion of the multimode region and intensity distribution upon the output throat (1.5×5 μm^2) demonstrates the high sensitivity of propagation to such changes.

Our considerations are limited to the MMI coupler with the following structure, $n_{\mathrm{MMI}} = 1.56$, $W_{\mathrm{MMI}} = 10$ μm, $d = 4.5$ μm, $b = 1.5$ μm and $\chi_e^{(3)} = 8.4\times10^{-18}$ m^2/W. These parameters show the core refractive index, effective width, transversal distance between the multimode waveguide center and the single input waveguide centers, input waveguides width, and third-order susceptibility, respectively.

Notably, the material used for the core layer is polydiacetylene due with high nonlinearity. This material is a Π-junction and has excellent nonlinear properties. Thus, its susceptibility is more than eight times bigger than that of silicon. Therefore, polydiacetylene may be best candidate to apply in the NLMMI coupler.

In this section, we present the results that show the ability of NLMMI to propose biological/chemical and geophysics sensors. The sequence of the results and discussion are shown as follows to give the reader logical purposes about the mentioned sensor.

The first parameter that should be determined is input intensity, which increases the sensitivity of the design. Hence, output intensity as a sensing operation parameter

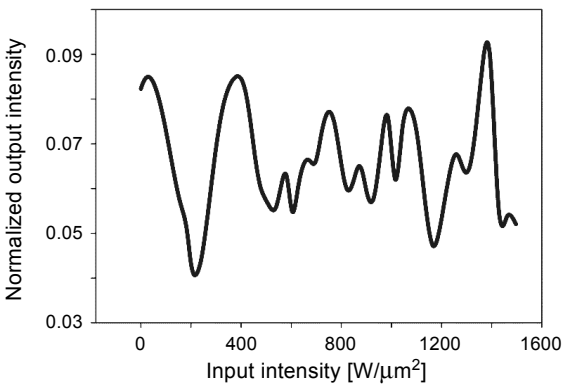

Fig. 4. Output intensity as a function of input intensity where the refractive contrast index is 0.56 and the wavelength is 1550 nm.

is studied as a function of input intensity, as shown in Fig. 4. The result shows oscillation on 1000 W/μm^2 (electric field is 7×10^8 N/C), which could be a good option for an input intensity candidate.

The output sensitivity to input wavelength is an inseparable element of our device; Fig. 5 validates our claim by studying the normalized output electric field and insertion loss as a function of input wavelength. This demonstration shows biological and geophysics sensors, as discussed below.

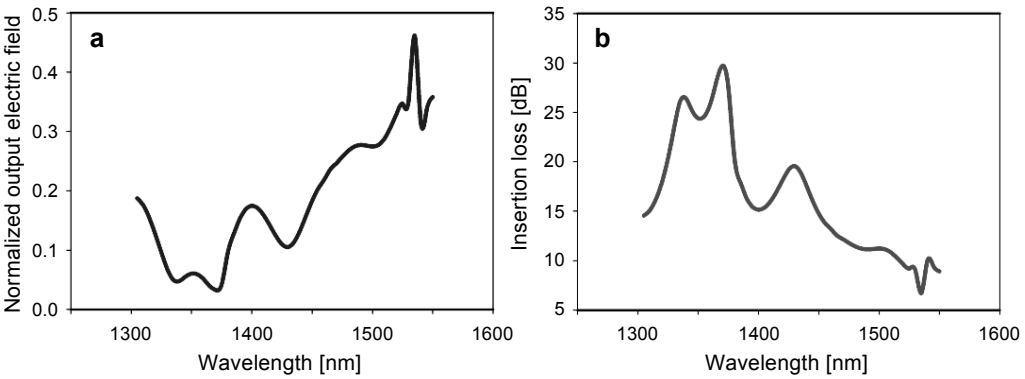

Fig. 5. Normalized output electric field (**a**) and insertion loss (**b**) as a function of input wavelength where $n_{clad} = 1$.

Several researchers claim that an input wavelength around 1550 nm is not a good option for sensing by polymer waveguides because of higher absorption on these wavelengths. As such, they choose 1300 nm as the input wavelength [9]. However, insertion losses in MMI waveguides are considerable in such cases compared with the absorption. In nonlinear regime, the result shows that the loss is lower around 1550 nm than 1300 nm, as shown in Fig. 5**b**. Therefore, 1550 nm can be feasible for a good sensor.

The sensitivity to input wavelength guides us to produce sensors that can detect earthquake, blood pressure, and heart waves. For clarity, we divided them into two categories: earthquake and body sensing.

When inputs are connected to the earth, an interaction with any wave such as an acoustic wave can affect the input wavelength and different wavelengths (or frequency) are shown to the NLMMI. High sensitivity to input wavelength enables the detection of earth waves such as earthquake waves. Notably, it can provide information sooner than implemented sensors. Furthermore, more applications could be proposed because of the sensitivity of the input wavelength to any kind of waves that also contain light. It can operate as a switch to automatically turn the lamps off and on at day or night. The reorganization between the words in spelling can be another application so that such sounds can be translated and converted to word codes during monitoring.

Body applications enable physicists to realize heart operation by touching the heart area with input waveguide. Putting an input waveguide on a vena enables the measurement of blood pressure and pulse numbers.

An important application of waveguide sensors are refractive sensors. In nonlinear regime, especially in multimode, the waveguide could demonstrate higher sensitivity to the cladding refractive index without the need of complicated structures. In this paper, we discuss air cladding and water cladding sensors.

First, we tested the refractive index in three different input wavelengths by studying the output intensity in air with a cladding on 1300, 1530, and 1550 nm. This test can give more insight for choosing a wavelength and for accurately measuring air pollution (Fig. 6).

Figure 6 demonstrates the output intensity of refractive index in air at 1550, 1530, and 1300 nm wavelengths. At 1530 nm, more oscillations are observed. As such, it can be a good candidature for air sensing.

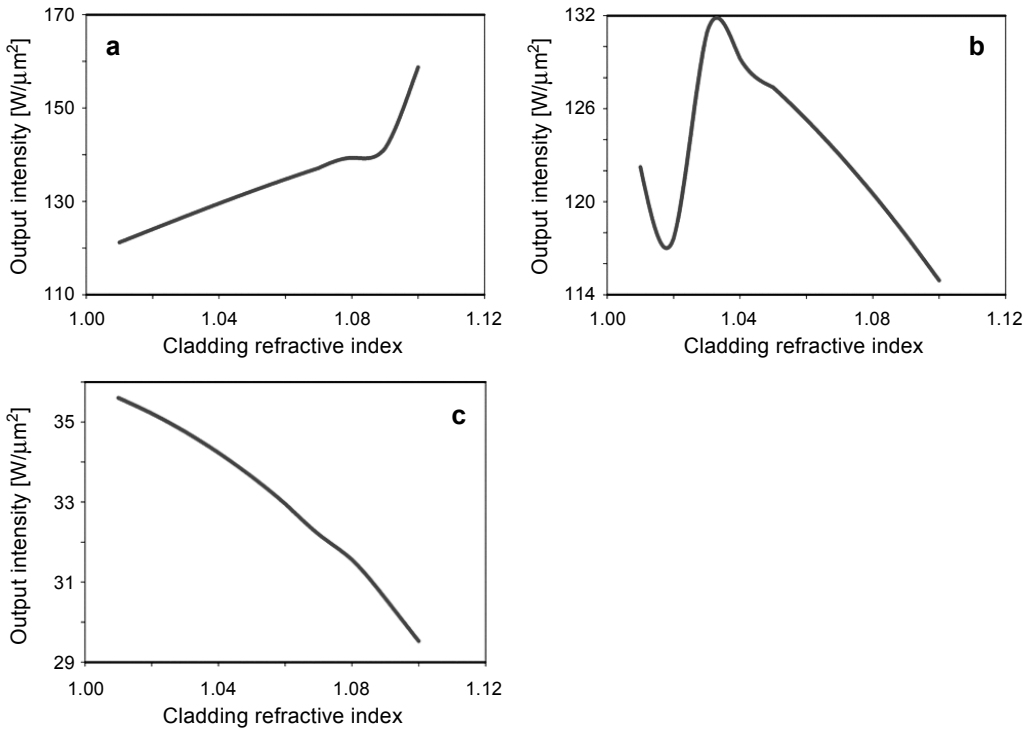

Fig. 6. Output intensity as a function of cladding refractive index in air where wavelength is 1550 nm (**a**), 1530 nm (**b**), and 1300 nm (**c**).

Several researchers prefer the linear curve because of its ability to relate any intensity to a special refractive index, which makes their work easy. However, the accuracy in the small slope is low, similar to that in 1300 nm. However, the linear curve can only detect just one type of pollution, such as detecting the density of carbon in air. Applying the wavelength with more oscillation while having multiple intensities for the refractive index remains to be a challenge. The answer is increasing the output numbers to analyze any point of refractive index and different amounts of intensity in

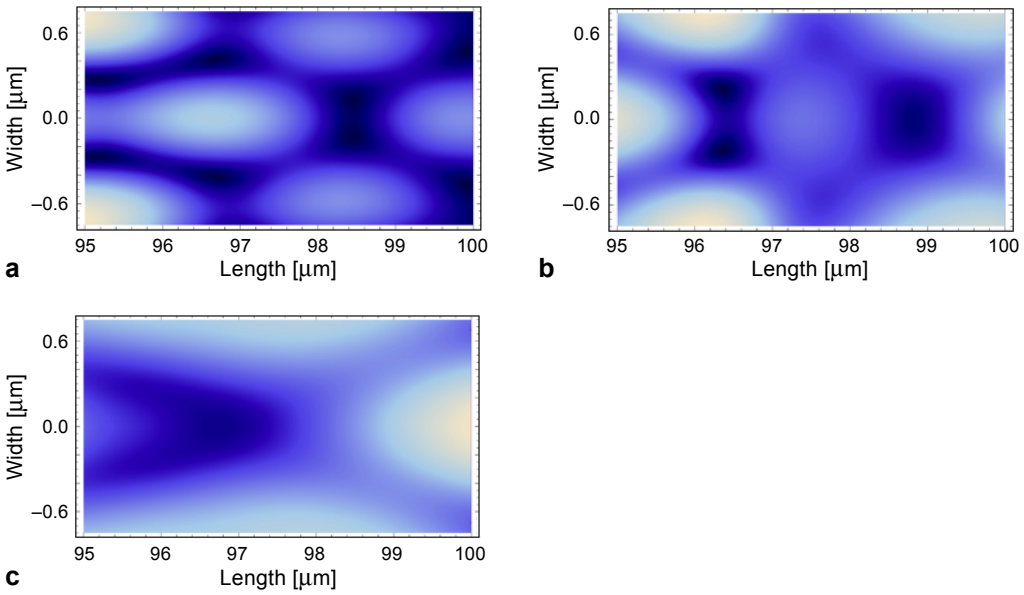

Fig. 7. Output throat at three wavelengths: 1300 nm (**a**), 1530 nm (**b**), and 1550 nm (**c**).

the outputs so that the pollution in air and water can be detected. Here, we choose 1530 nm because it has a higher slope than other wavelengths.

The intensity distributions in the throat of an output facet show that 1530 nm is the best choice, as shown in Fig. 7. These simulated results are also provided in Fig. 6. Three spots in **b** explain the capability of 1530 nm to detect with high accuracy.

The use of water-soluble refractive index range is the best candidate in sensing chemically and biologically. Therefore, we apply our design at 1530 nm of wavelength in the range of 1.3 to 1.5 cladding refractive indices. The result is shown in Fig. 8 and

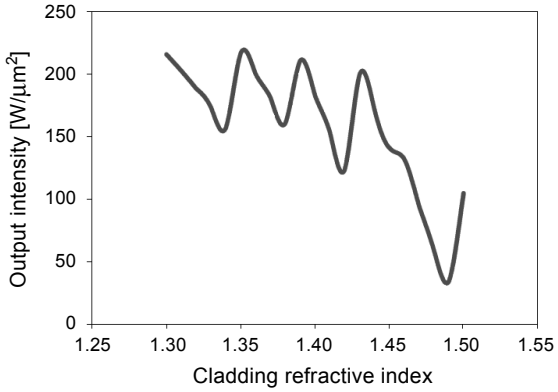

Fig. 8. Output intensity as a function of cladding refractive index in the range of 1.3 to 1.5 where the wavelength is 1530 nm.

demonstrates that a high oscillation is observed in the output intensity in the mentioned range. Therefore, the percentage of five or more soluble components, such as sugar, protein, and so on, can be detected with high accuracy.

Another application of our device is for blood testing, especially in detecting blood parameters. Such a test could be done in less than a second, and this sensor might be used in blood tests and in photonics sensing in biological/chemical science in the future.

Mode interferences are based on multimode interferences that become stronger in a nonlinear regime because of cross-phase modulation and wave-mixing effects. Here, the contribution of cladding refractive index to interference is discussed. Therefore, we indicate the intensity distribution in particular cladding layers in ranges of air and water.

Here, the simulated result shows different mode expansions and output throat distributions on six clad layers, as shown in Figs. 9 and 10, respectively.

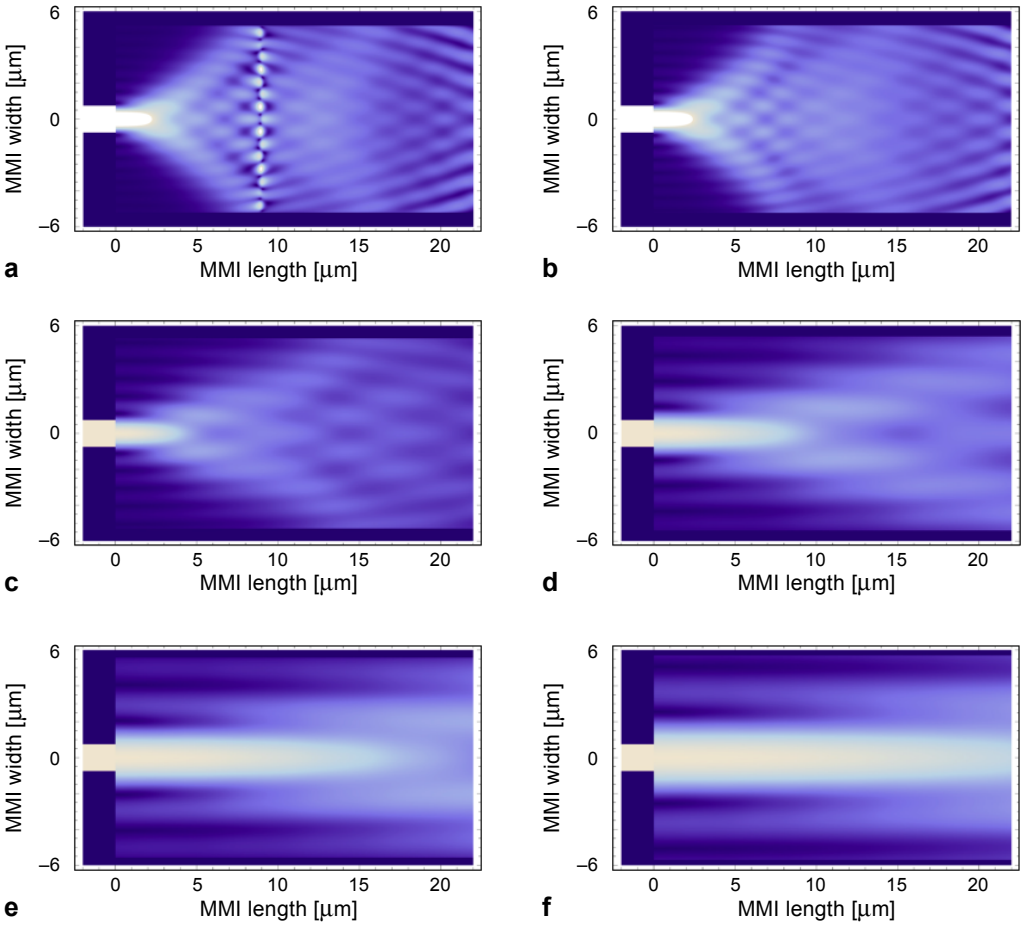

Fig. 9. Field distribution where the cladding refractive index is 1 (**a**), 1.1 (**b**), 1.33 (**c**), 1.44 (**d**), and 1.5 (**e**).

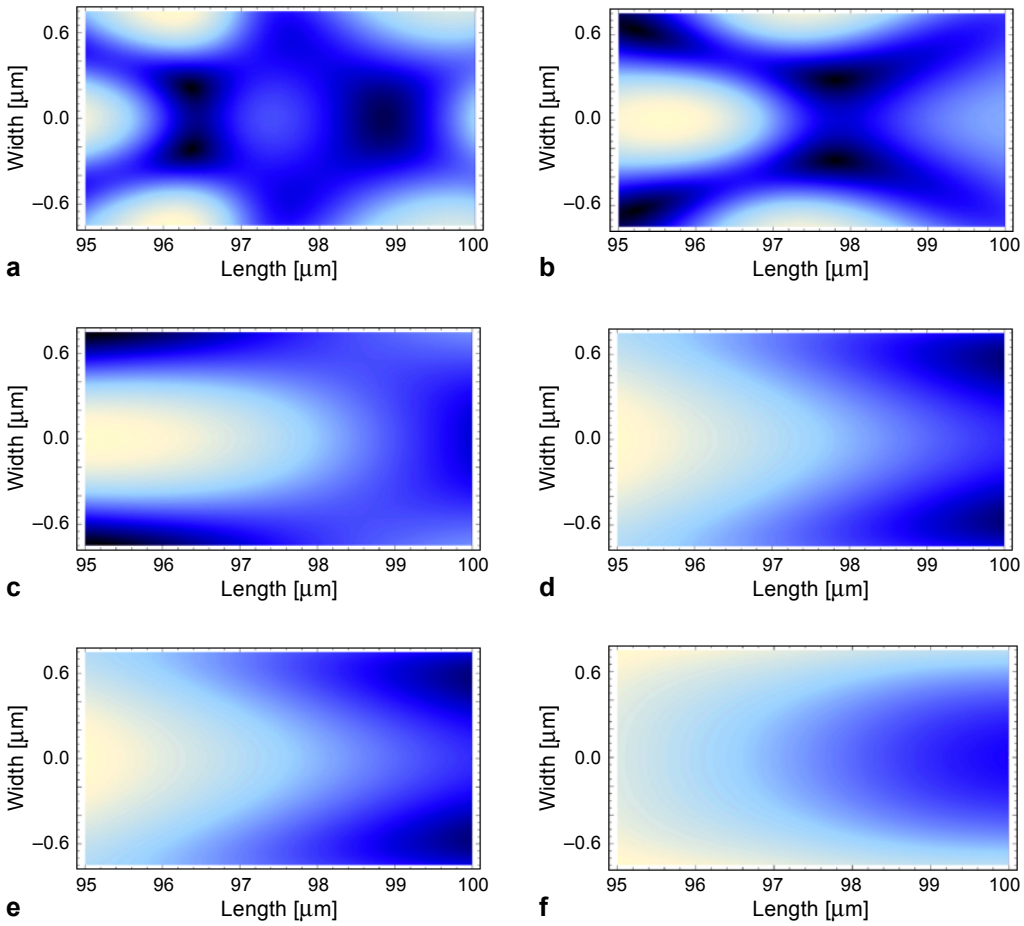

Fig. 10. Output throat on six clad layers.

The simulated results on the last two figures demonstrate high detection of the proposed sensor by NLMMI because of the reaction to small changes in the cladding refractive index.

Notably, in this paper, we focus on a general explanation to show the ability of NLMMI based on NMPA to produce a high accuracy sensor with a broad range of applications.

4. Conclusions

We propose an all-optical sensor based on NMPA in an MMI coupler. The sensor can be tuned to have the highest sensitivity in refractive index ranges sufficient to detect water-soluble chemical or biological materials and air pollution. Moreover, our device could be used as a seismograph because of the reaction to changes in input wavelength. The Kerr nonlinear effect is studied to produce the high-efficiency sensor so that it can

be operated on any choice of materials for waveguide. Even conventional glass can be used to design the sensor. The results show visible changes in the field distribution in the MMI region with the refractive index and input wavelength of various surrounding layers, which show high sensitivity to the mentioned parameters to propose biological/ chemical and wave sensors.

In our future work, we are going to consider the number of outputs same as the number of oscillation and work on a spatial sensor that can detect air pollution or protein, fat, urea, sugar, cholesterol, and bacteria in blood sensors. Other options might include sensing earthquake and heart pulses.

Acknowledgments – This research project was funded by the University Sains Malaysia Research University Grant No. 1001/PFIZIK/811220, Education Ministry FRGS Grant No. 203/PFIZIK/6711349, and the Department of Higher Education Exploratory Research ERGS Grant No. 203/PFIZIK/6720051.

References

[1] Soldano L.B., Pennings E.C.M., *Optical multi-mode interference devices based on self-imaging: principles and applications*, Journal of Lightwave Technology **13**(4), 1995, pp. 615–627.

[2] Heliang Liu, Hwayaw Tam, Wai P.K.A., Pun E., *Low-loss waveguide crossing using a multimode interference structure*, Optics Communications **241**(1–3), 2004, pp. 99–104.

[3] Besse P.A., Bachmann M., Melchior H., Soldano L.B., Smit M.K., *Optical bandwidth and fabrication tolerances of multimode interference couplers*, Journal of Lightwave Technology **12**(6), 1994, pp. 1004–1009.

[4] Qian Wang, Ho S.T., *Ultracompact multimode interference coupler designed by parallel particle swarm optimization with parallel finite-difference time-domain*, Journal of Lightwave Technology **28**(9), 2010, pp. 1298–1304.

[5] Agashe S.S., Shiu K.-T., Forrest S.S., *Compact polarization insensitive InGaAsP-InP 2×2 optical switch*, IEEE Photonics Technology Letters **17**(1), 2005, pp. 52–54.

[6] Jung Moo Hong, Hyun Ho Ryu, Soon Ryong Park, Jae Wan Jeong, Seung Gol Lee, El-Hang Lee, Se-Geun Park, Deokha Woo, Sunho Kim, Beom-Hoan O, *Design and fabrication of a significantly shortened multimode interference coupler for polarization splitter application*, IEEE Photonics Technology Letters **15**(1), 2003, pp. 72–74.

[7] Szewczuk A., Błahut M., *Multimode interference structures of variable geometry for optical sensor application*, Acta Physica Polonica A **118**(6), 2010, pp. 1254–1258.

[8] Dooyoung Hah, Euisik Yoon, Songcheol Hong, *An optomechanical pressure sensor using multimode interference couplers with polymer waveguides on this p^+-Si membrane*, Sensors and Actuators A: Physical **79**(3), 2000, pp. 204–210.

[9] Mayeh M., Viegas J., Srinivasan P., Marques P., Santos J.L., Johnson E.G., Farahi F., *Design and fabrication of slotted multimode interference devices for chemical and biological sensing*, Journal of Sensors, Vol. 2009, 2009, article 470175.

[10] Tajaldini M., Jafri M.Z.M., *Nonlinear modal propagation analysis method in multimode interference coupler for operation development*, AIP Conference Proceedings **1528**, 2013, p. 450.

[11] Tajaldini M., Jafri M.Z.M., *The influence of nonlinear modal propagation analysis on MMI power splitters for miniaturization*, Proceedings of SPIE **8789**, 2013, article 87890P.

[12] Tajaldini M., Jafri M.Z.M., *Proposal of a novel method for all optical switching with MMI coupler*, Proceedings of SPIE **8545**, 2012, article 854505.

[13] Tajaldini M., Jafri M.Z.M., *Simulation of an ultra-compact multimode interference power splitter based on Kerr nonlinear effect*, Journal of Lightwave Technology **32**(7), 2014, pp. 1282–1289.

[14] TAJALDINI M., JAFRI M.Z.M., *Ultra compact 1×11 power splitter using polydiacetylene multimode interference coupler*, Advanced Materials Research **626**, 2013, pp. 853–860.
[15] TAJALDINI M., JAFRI M.Z.M., *An ultra-compact multimode interference coupler as an optimum all-optical switch based on nonlinear modal propagation analysis*, Optics Communications **324**, 2014, pp. 85–92.
[16] EULISS G., *Temporal characteristics and scaling considerations of multimode interference couplers*, Journal of Lightwave Technology **17**(7), 1999, pp. 1206–1210.

Received March 7, 2015